International Journal of Biological Macromolecules 320 (2025) 144779

Contents lists available at ScienceDirect

International Journal of Biological Macromolecules

journal homepage: www.elsevier.com/locate/ijbiomac

Fabrication of zirconium/chitosan functionalized magnetic carbon nanotubes for enhanced adsorption of alizarin red

Jing Jin [a], Hanyu Zhang [a], Aaron Albert Aryee [a,b], Yuanyuan Wang [a], Rashda safdar [a], Weimin Shi [a,*], Lingbo Qu [a], Runping Han [a,*]

[a] College of Chemistry, Zhengzhou University, Kexue Dadao #100, Zhengzhou 450001, China
[b] Department of Chemistry, College of Basic and Applied Sciences, University of Ghana, Legon, Ghana

ARTICLE INFO

Keywords:
Magnetic carbon nanotubes
Chitosan
Zirconium
Adsorption
Alizarin red

ABSTRACT

In this study, a composite adsorbent (Zr-CMCNTs) based on modification of magnetic carbon nanotubes (MCNTs) with chitosan (CS) and zirconium oxychloride octahydrate ($ZrOCl_2 \cdot 8H_2O$) was synthesized and showed excellent adsorption ability for alizarin red (AR) in aqueous solution. The maximum adsorption capacity of Zr-CMCNTs for AR could reach 889 $mg \cdot g^{-1}$ at 313 K (pH = 3.4). The performance was not significantly affected by the presence of common ions, showing good salt tolerance. The adsorption equilibrium process was consistent with Langmuir, Freundlich, Koble-Corrigan, and Temkin models, suggesting that both monolayer and multilayer adsorption were involved. The adsorption kinetic process was well described by the pseudo-second-order, Elovich and Double constant kinetic models. The thermodynamic parameters calculated confirm the adsorption process to be spontaneous, endothermic and entropy-increasing. Analyses of the underlying mechanism shows that the adsorption process was mainly due to complexation, hydrogen bonding, π-π stacking and electrostatic attraction. The magnetic property enables Zr-CMCNTs to be recovered easily following adsorption. After three desorption and regeneration cycles, the removal rate of AR still reached 60 %, indicating good reusability. Overall, Zr-CMCNTs composite adsorbent shows great potential in dye wastewater treatment.

1. Introduction

Access to clean water is of immense importance to life on earth. However, with the rapid development of society and the acceleration of industrialization, the pollution of water bodies is on the rise leading to a global shortage of water resources [1]. According to the United Nations Environment Program, half of the world's population is still expected to be under pressure from water shortages by 2030 [2]. To date, only 10 % of China's water resources meet drinking water sanitation standards, and the national water resource pollution rate is as high as 50 % [3]. There is a wide variety of pollutants in water bodies, including phenols, pharmaceuticals and personal care products (PPCPs), pesticides, dyes, etc. These pollutants are discharged into water bodies through chemical industries and agricultural activities, exceeding the self-purification capacity of the environment, deteriorating the water environment and posing a serious threat to water body ecology and human health [4]. Therefore, the control and management of water pollution issues more effectively is of utmost priority.

Dyes are refractory organic pollutants that are highly resistant to chemical and biological degradation due to their complex aromatic structures. Dyes stain water bodies, affect water transparency and reduce the oxygen content of water bodies, thus affecting aquatic biological systems. Additionally, most of the dyes are toxic, mutagenic and carcinogenic and can be harmful to aquatic organisms, microorganisms and human health [5]. They can be classified as anthraquinone dyes, acid dyes, basic dyes, azo dyes, reactive dyes, disperse dyes and metal complex dyes according to their structure [6]. Anthraquinone dyes have a stable conjugated structure, high chromaticity, complex composition, and are difficult to oxidize and degrade [7]. Alizarin red (AR), as an anthraquinone dye, is widely used in acid-base indicators, nylon and wool dyeing.AR has a special aromatic structure, is highly toxic and difficult to degrade. Therefore, it is necessary to select an effective method to remove AR from dye wastewater in order to reduce its harm to the water environment, plants and animals.

The adsorption method has been extensively studied for the remediation of dye wastewater [8]. Because it has the advantages of a wide

---

* Corresponding authors.
E-mail addresses: shiweimin@zzu.edu.cn (W. Shi), qulingbo@zzu.edu.cn (L. Qu), rphan67@zzu.edu.cn (R. Han).

https://doi.org/10.1016/j.ijbiomac.2025.144779
Received 12 March 2025; Received in revised form 24 May 2025; Accepted 28 May 2025
Available online 28 May 2025
0141-8130/© 2025 Elsevier B.V. All rights are reserved, including those for text and data mining, AI training, and similar technologies.

range of adsorbents to be choosen, simplicity of operation, high efficiency and low cost [9]. Carbon nanotubes (which are categorized into single-walled carbon nanotubes and multi-walled carbon nanotubes), a highly versatile carbon nanomaterial, have been widely used in wastewater treatment because of their excellent thermal and chemical stability, as well as their large specific surface area and high porosity. However, carbon nanotubes are hydrophobic, therefore easy to agglomerate in aqueous solution, which hinders its application in waters. Meanwhile, the pristine carbon nanotubes have limited adsorption capacity to ionic pollutants even with superior surface property [10]. To overcome this shortcoming, functional groups could be introduced into carbon nanotubes to not only enhance hydrophilicity but also provide better adsorption ability. For example, pentaerythritol was utilized to modify multi-walled carbon nanotubes for removing alizarin yellow R (AYR) and alizarin red S (ARS) [11]. Carbon nanotubes functionalize with ionic liquids showed improved adsorption capacity for sulfamethoxazole and ketoprofen [12]. Fabrication of magnetic carbon nanotubes is another advance in its application in wastewater treatment study, because it proves easy operation for recovery [13,14]. Foroutan [15] et al. prepared CNT/MgO/$CuFe_2O_4$ magnetic composites using co-precipitation method. The composites showed good adsorption capacity for methyl violet and Nile blue dyes with maximum adsorption of 36.5 and 35.6 $mg{\cdot}g^{-1}$, respectively, and the materials remained good after five cycle regeneration experiments.

Although the addition of magnetism enables CNTs to obtain easy recovery, the magnetic loading may cover the functional groups on CNTs and reduce the inherent adsorption performance of CNTs. CNTs have a large specific surface area and a hollow internal structure, in addition, the direct presence of conjugated large π-bonds in the carbon atoms of CNTs gives them an aromatic nature, which is favorable for π-π interactions. Therefore, polymers can be used to modify CNTs so as to introduce various functional groups to meet the requirements of adsorption of organic pollutants in wastewater [16]. Maithili et al. [17] prepared glutaraldehyde cross-linked chitosan-alginate composite [(Cs-F-An)-G-Al] for the removal of Brilliant green, Methyl orange, and Patent Blue V from dye wastewater. The maximum adsorption capacities were 235.82, 198.09 and 117.34 $mg{\cdot}g^{-1}$, respectively. The adsorption mechanism was dominated by chemical adsorption, involving ion exchange, hydrogen bonding, and complexation. Specifically, glutaraldehyde served as a cross-linking agent to react with the amino groups of chitosan, forming Schiff bases (-C=N-), which covalently connected chitosan and alginate to create a stable network structure. This structure enhanced the chemical stability of the composite material, preventing swelling or decomposition in aqueous solutions. Additionally, the Schiff bases provided additional adsorption sites, which could assist in capturing dye molecules through weak electrostatic interactions or coordination effects. In addition, chitosan has great potential for the treatment of industrial wastewater, especially dye wastewater [18,19].

Transition metals such as zirconium (Zr), iron (Fe), lanthanum (La), and nickel (Ni) can form ligands with some pollutants through complexation. Hence transition metals can be utilized to modify carbon nanotubes so as to improve their adsorption performance for anionic pollutants. Gu et al. [20] prepared zirconium-modified carbon nanotubes (Zr-CNTs) adsorbents using zirconium oxychloride octahydrate ($ZrOCl_2{\cdot}8H_2O$) impregnated carbon nanotubes for batch removal of PO_4^{3-} from solution. Zr-CNTs exhibited excellent PO_4^{3-} adsorption performance, which was mainly due to the presence of complexation in the adsorption process. After multiple desorption and regeneration, the material still retained strong adsorption capacity.

Based on the above studies, multiple modifications might be the ultimate solution for adsorbent development. At the same time, multiple-layer design should improve the stability of CNTs-based materials, therefore decrease metal leaching from the synthesized materials during application [21]. In this study, multi-walled carbon nanotubes (CNTs) were used as raw materials to synthesize magnetic materials (labeled as MCNTs) by the co-precipitation method. To further improve its adsorption ability, chitosan (CS) was incorporated into its structure via the cross-linking deposition method and the resulting material labeled as CMCNTs. To enhance its selectivity on anionic pollutants even further, this composite material was impregnated with Zr using zirconium oxychloride octahydrate ($ZrOCl_2{\cdot}8H_2O$) to form the composite labeled as Zr-CMCNTs. This synthetic design is expected to furnish the composite with high efficiency and reusability towards the removal of alizarin red.

2. Materials and research methods

2.1. Experimental reagents

The main reagents in this experiment were industrial-grade multi-walled carbon nanotubes (CNTs), chitosan (CS), zirconium oxychloride octahydrate ($ZrOCl_2{\cdot}8H_2O$), ferric chloride hexahydrate ($FeCl_3{\cdot}6H_2O$), ferrous sulfate heptahydrate ($FeSO_4{\cdot}7H_2O$), ethanol (C_2H_5OH), glacial acetic acid (CH_3COOH), glutaraldehyde ($C_2H_8O_2$), hydrochloric acid (HCl), sodium hydroxide (NaOH), sodium chloride (NaCl), anhydrous calcium chloride ($CaCl_2$), anhydrous sodium sulfate (Na_2SO_4), alizarin red (AR), acidic chrome blue K (AK), and water. The main reagents used are listed in Table S1.

2.2. Preparation of MCNTs

Firstly, 1.00 g CNTs were weighed in a 500 mL beaker, and 3.22 g of $FeCl_3{\cdot}6H_2O$, 1.66 g $FeSO_4{\cdot}7H_2O$ and 200 mL of distilled water added. The beaker with its contents was subjected to ultrasonic treatment for 30 min at room temperature to form a homogeneous mixture. The pH of this solution was adjusted to about 11 by slowly adding 1 $mol{\cdot}L^{-1}$ NaOH solution, after which the beaker was transferred into a magnetic stirring water bath at 90 °C for 30 min. After completion, it was taken out and washed repeatedly with distilled water until it reached neutrality. Finally, the MCNTs were dried in an oven at 60 °C and milled to obtain the MCNTs materials [22]. Fig. S1(A) shows the synthetic procedure for MCNTs.

2.3. Preparation of CMCNTs

1.00 g of CS was weighed in a 500 mL beaker containing 200 mL of 4 % acetic acid solution. About 1.00 g of MCNTs was then added and the solution ultrasonicated for 30 min at room temperature to make the mixture homogeneous. The mixed solution was placed in a magnetic stirring water bath at 40 °C, and 1 mL of 50 % glutaraldehyde solution added. The reaction was aged for 1 h after which 1 $mol{\cdot}L^{-1}$ NaOH solution was added slowly to adjust the pH to 10. The temperature of the water bath was then raised to 70 °C and the reaction allowed to proceed for 2 h. After the reaction, the beaker was taken out and left to cool to room temperature. The uncross-linked CS on the surface of the material was first washed with 0.5 % acetic acid solution, and then washed repeatedly with distilled water and anhydrous ethanol until the filtrate reached neutrality. Finally, it was dried in an oven at 60 °C and then ground to obtain the CMCNTs material [23]. Fig. S1(B) shows the schematic diagram of the preparation of CMCNTs.

2.4. Preparation of Zr-CMCNTs

2.00 g of $ZrOCl_2{\cdot}8H_2O$ was weighed into a 500 mL beaker and 200 mL of distilled water added to fully dissolve it after which 1.00 g of CMCNTs was added, and then magnetically stirred for 6 h at 30 °C. After completion, it was taken out and washed repeatedly with distilled water until it reached neutrality. Finally, the Zr-CMCNTs materials were dried in a constant temperature oven at 60 °C overnight. After this period, the material was obtained and placed in an air-tight container [24]. Fig. S1 (C) shows the schematic diagram for the preparation of Zr-CMCNTs.

2.5. Characterization of materials

The adsorbent materials were characterized to understand their surface morphology and synthesis mechanism. In order to understand the surface electrical properties of the adsorbent, the composites were subjected to the determination of the isoelectric point. Scanning electron microscopy was used to observe the morphological changes of CNTs before and after modification. The synthesized materials were analyzed using infrared spectroscopy to compare the differences in the surface functional groups of CNTs before and after modification. N_2 adsorption and desorption tests were performed on the materials before and after modification to compare their specific surface area size. The vibrating sample magnetometer technique was used to determine the magnetization strength and the type of hysteresis loop of the materials. Thermogravimetric analysis of the adsorbed materials was performed to determine the composition of the materials. To investigate the stability of the adsorbent in solution, the leaching rates of the metals Fe and Zr in solution at different pH were determined.

2.6. Adsorption experiments

The static adsorption experiments were carried out in a thermostatic shaking chamber at 303 K at an agitation speed of 120 rpm. The experiments focused on the effects of different conditions such as contact time, pH, adsorbent dosage, and salt concentration on the adsorption process. The concentration of the solution remaining after adsorption studies was measured during the experiment and the removal rate p and unit adsorption q of the adsorbent for the adsorbent were calculated according to Eqs. (1) and (2) respectively. Adsorption isotherms and adsorption kinetics experiments were used to select a suitable model to describe the adsorption process as well as explore the underlying mechanism. The influence of temperature was further assessed and the associated thermodynamics parameters determined accordingly.

$$p = \frac{C_0 - C_t}{C_0} \times 100\% \tag{1}$$

$$q = \frac{V(C_0 - C)}{m} \tag{2}$$

where p is the removal rate of adsorbent (%), C_0 is the initial concentration of adsorbent ($mg \cdot L^{-1}$), C_t is the concentration in the solution after adsorption equilibrium ($mg \cdot L^{-1}$), q is the adsorbed amount (q_t or q_e, $mg \cdot g^{-1}$), m is the mass of adsorbent (g), and V is the volume of the solution (L).

2.7. Desorption and regeneration

In order to explore the regeneration ability of the adsorbents in the experiments, the desorption and regeneration experiments of the adsorbents were carried out by using eluents such as ethanol, sodium hydroxide, hydrochloric acid, salt and deionized water, respectively. In this study, the AR-loaded adsorbents were obtained from the adsorption study as described above. The amount of dye adsorbed at equilibrium for the first adsorption cycle was measured and recorded as q_0. After washing and drying with deionized water, various eluting solutions were added for desorption and the mass of desorbed adsorbent recorded as m_d. After washing and drying, the adsorbent was put into the adsorbent solution again and adsorbed until saturation was reached. According to the desorption and regeneration results, a suitable desorption solution was selected for three cycle experiments, and the desorption rate d and regeneration rate r were calculated as shown below:

$$d = \frac{m_d}{m_0} \times 100\% \tag{3}$$

$$r = \frac{q_n}{q_0} \times 100\% \tag{4}$$

where q_0 is the amount of adsorption that reaches saturation for the first adsorption ($mg \cdot g^{-1}$), q_n denotes the amount of adsorption that reaches saturation for adsorption ($mg \cdot g^{-1}$), m_0 is the mass of adsorbate before desorption of the adsorbent (mg), and m_n the mass of adsorbate desorbed off (mg).

3. Results and discussion

3.1. Characterization of materials

3.1.1. Analysis of zero point charge (pH_{pzc})

From Fig. S2, the isoelectric point of Fe_3O_4 and CNTs were 6.44 and 6.55. After modification the isoelectric point of MCNTs was 6.44 and that of CMCNTs was 6.61. The increase in the value of isoelectric point after modification may be due to the introduction of the alkaline functional group -NH_2 into the material [25]. The functional group underwent dissociation which resulted in the shift of isoelectric point to the right [26].The isoelectric point of Zr-CMCNTs was 4.65, suggesting s shift towards acidic region after modification. This may be due to the fact that after $ZrOCl_2 \cdot 8H_2O$ modification, ZrO(II) was loaded onto the material in complex form. In this process, the basic functional groups decreased while the zirconia acidic groups increased accordingly [27].

3.1.2. Scanning Electron microscope analysis

Scanning electron microscopy (SEM) was used to analyze and observe the morphological changes of CNTs before and after modification. Fig. 1 shows the SEM image of CNTs, MCNTs, CMCNTs and Zr-CMCNTs. From Fig. 1a, it can be seen that the CNTs possessed regular tubular structures, which have relatively smooth surfaces and do not contain other substances. From Fig. 1(b, c, d), it can be observed that relative to the CNTs, the surface of the materials become rougher, but without changing its original tubular structure. Fig. 1b shows MCNTs with relatively rough surface and the presence of a large number of Fe_3O_4 metal particles deposited in it. The surface of CMCNTs in Fig. 1(c) is wrapped by CS and becomes rougher [28], but the structure is relatively loose. In Fig. 1(d), it was found that the $ZrOCl_2 \cdot 8H_2O$ modification resulted in a denser structure and richer surface of Zr-CMCNTs. The combined specific surface area gradually decreased, indicating that the three composites were successfully prepared.

3.1.3. FT-IR analysis

In order to compare the differences in the surface functional groups of CNTs before and after modification, the FT-IR spectrum of the synthesized materials was analyzed and the results shown in Fig. 2. As can be seen from Fig. 2, the modified CNTs all showed Fe—O stretching vibrations near 598 cm^{-1}, indicating that the modified adsorbents are all magnetic [29]. Fig. 2(b, c, d) showed that there is a broad peak near 3446 cm^{-1} which is the peak of O—H, N—H stretching vibration, indicating that the CMCNTs were prepared successfully [30,31]. After CS modification, the intensity of the stretching vibration peak located near 3446 cm^{-1} was enhanced, while the characteristic peak at 2922 cm^{-1} was attributed to the stretching vibration of C—H [32], and the vibrational peak of C—N appeared near 1635 cm^{-1} [33], indicating that the CS modification was successful, which resulted in the adsorbent CMCNTs containing abundant –NH_2 and –OH functional groups. Fig. 2 revealed that the vibrational peaks at 3446 cm^{-1} and 1635 cm^{-1} were obviously reduced, and the C—O vibrational peak at 1072 cm^{-1} moved to 1000 cm^{-1}. This can be ascribed to the complexation of the –NH_2 and –OH functional groups in the CMCNTs with zirconia groups, indicating that the composite material Zr-CMCNTs was successfully prepared [34].

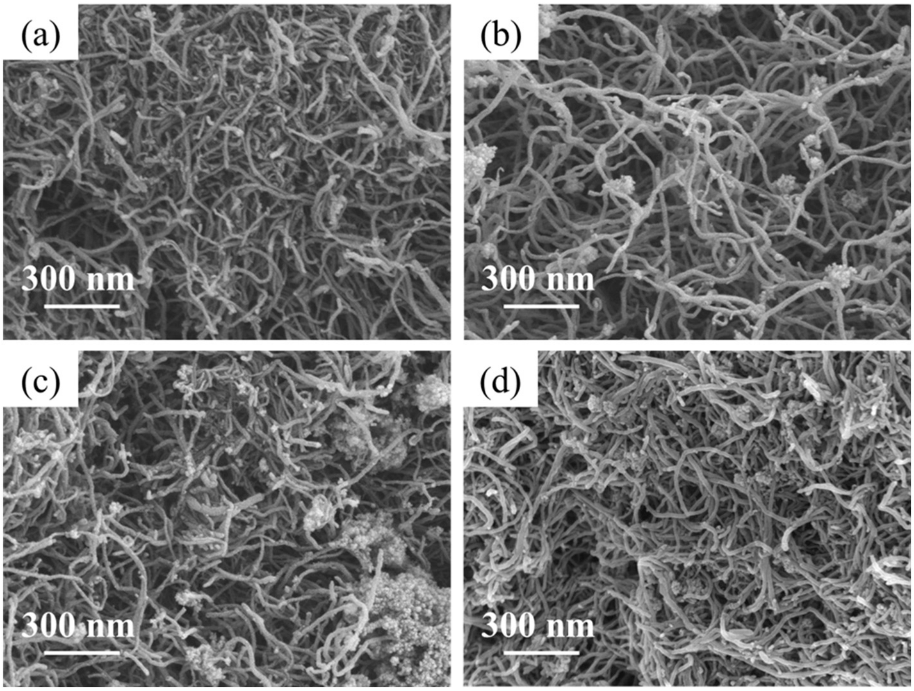

Fig. 1. SEM image of (a) CNTs, (b) MCNTs, (c) CMCNTs, and (d) Zr-CMCNTs. (Magnification: ×30,000; scale bar:300 nm).

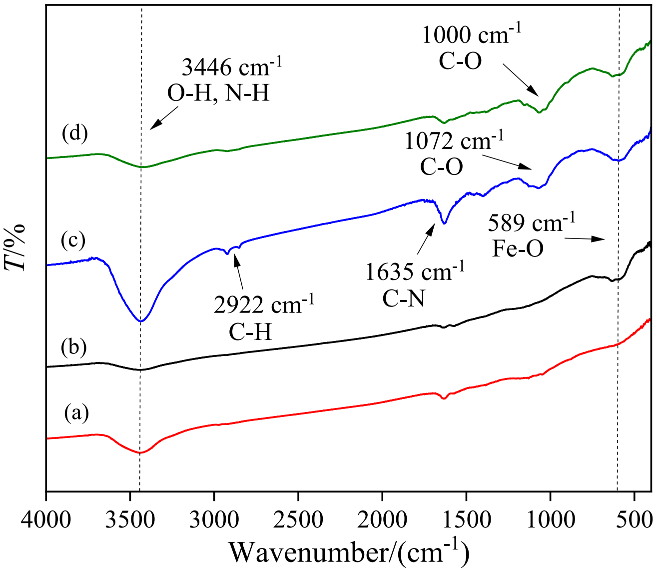

Fig. 2. FT-IR plots of adsorbents before and after modification (a. CNTs, b. MCNTs, c. CMCNTs, d. Zr-CMCNTs).

3.1.4. BET analysis

N_2 adsorption and desorption tests were carried out on the materials before and after modification, as shown in Fig. 3. Conferring to IUPAC classification, no obvious saturated adsorption plateau was observed for the four materials, CNTs, MCNTs, CMCNTs and Zr-CMCNTs, and the adsorption-desorption curves belong to the class IV isotherm [35,36]. All materials showed H3-type hysteresis loops in the relative pressure (P/P_0) range of 0.8 to 1.0. H3-type hysteresis loops were usually associated with slit pores formed by the accumulation of lamellar or layered particles. The width of the H3-type hysteresis loop gradually decreases in the modified material, indicating an increase in the irregularity of the mesoporous structure or a gradual filling of the pores. This is consistent with the rough, inhomogeneous surface results observed by SEM after chitosan cross-linking and loading with zirconium. Table 1 shows the specific surface area of the four materials. After CNTs were loaded with Fe_3O_4, Fe_3O_4 occupied part of the active sites and the specific surface area of MCNTs decreased. After CS modification, the specific surface area of CMCNTs decreased due to CS wrapped around the surface of MCNTs, which hindered the adsorption of N_2 [37]. After $ZrOCl_2{\cdot}8H_2O$ modification, the CMCNTs formed coordination with zirconium oxide groups, and the specific surface area further decreased.

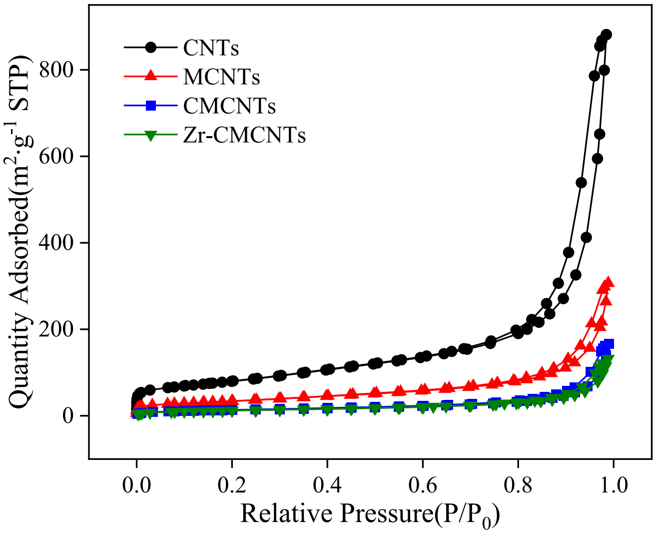

Fig. 3. BET plots of CNTs, MCNTs, CMCNTs and Zr-CMCNTs.

Table 1
Specific surface area of CNTs, MCNTs, CMCNTs and Zr-CMCNTs.

Sample	CNTs	MCNTs	CMCNTs	Zr-CMCNTs
BET Surface Area ($m^2{\cdot}g^{-1}$)	274	119	47.9	44.0

3.1.5. *XRD analysis*

XRD tests were carried out to explore the crystalline structure of the modified carbon nanotube materials and the results are shown in Fig. 4. From Fig. 4, it can be seen that the characteristic diffraction peaks belonging to Fe_3O_4 (JCPDS 75–0449) which appeared at $2\theta = 30.2°$, 35.8°, 43.5°, 57.3° and 62.3° for the studied materials correspond to the five crystal planes of Fe_3O_4. The characteristic diffraction peaks of CNTs appeared at $2\theta = 25.9°$, indicating that Fe_3O_4 was successfully loaded onto CNTs and that the composites were all magnetic. With each modification, the peak shape of the material did not change, but the peak intensity was weakened, indicating that the crystalline shape of the modified composites did not change. The magnetic properties are weakened, which is consistent with the VSM characterization results.

3.1.6. *VSM analysis*

The vibrating sample magnetometer (VSM) technique was used to determine the magnetization strength and the type of hysteresis loop of the materials. From Fig. S3(A), the magnetization strengths of Fe_3O_4, MCNTs, CMCNTs, and Zr-CMCNTs were 64.1 $emu \cdot g^{-1}$, 23.8 $emu \cdot g^{-1}$, 11.7 $emu \cdot g^{-1}$, and 9.11 $emu \cdot g^{-1}$, respectively. With the continuous modification of CNTs, the magnetization strength of the prepared materials gradually decreased and the magnetic properties became weaker [38]. This might be attributed to the introduction of chitosan and Zr diluting the magnetic components and reducing their proportion, while they may also cover the surface of Fe_3O_4, hindering the complete response of its magnetic moments. Nevertheless, Zr-CMCNTs still exhibit high responsiveness to an applied magnetic field and can be separated and recovered via magnetic separation technology. From Fig. S3(B), the residual magnetism and coercivity of the material were obtained near 0, which belongs to the phenomenon of soft magnetic materials, indicating that the material is paramagnetic [39].

3.1.7. *Thermogravimetry analysis (TGA)*

TGA analysis was performed on the material to determine their composition and the results shown in Fig. S4. As shown in Fig. S4(a, b), the mass of the composites did not change significantly at $T < 500$ °C. When 500 °C $< T <$ 700 °C, the weight loss of CNTs and MCNTs was 98.2 % and 60.8 %, respectively. This shows that the mass loss of MCNTs was greater, which was due to the residual Fe_3O_4 of the material that could not be thermally decomposed after the combustion of carbon nanotubes. Fig. S4(c, d) shows that CMCNTs and Zr-CMCNTs exhibited multistage weight loss, which was mainly divided into three stages: dehydration, decomposition, and combustion. At $T < 200$ °C, the free and bound water in the composite gradually disappeared, and the functional groups $-NH_2$ and –OH in CS were gradually pyrolyzed [40]. At $T > 200$ °C, CS gradually decomposed, and around 300 °C, CS began to burn, and the quality of the composite material continued to decline [41]. When the carbon nanotubes burned at 500 °C < T < 700 °C, Fe_3O_4 was left in all materials, and the mass loss of CMCNTs and Zr-CMCNTs was 80.1 % and 78.5 %, respectively, which was 19.3 % and 17.7 % more than that of MCNTs. All four materials experienced significant structural collapse only after 300 °C, indicating that the materials all have good thermal stability.

3.1.8. *Metal leaching experiment*

In order to investigate the stability of the adsorbent in solution, the leaching rates of the metals Fe and Zr were determined in solution at different pH. As can be seen from Fig. S5, the leaching rate of metals is lower with the increase of pH. In the pH range of 2–11, only a very small amount of metal precipitation under acidic conditions was observed with the leaching rate <3 % for the studied metals. This indicates that the adsorbent has a wide range of pH applicability and good water stability.

3.2. *Adsorption study*

3.2.1. *Comparison of adsorption performance before and after modification*

In this study, 10 mg of Fe_3O_4, CNTs, MCNTs, CMCNTs and Zr-CMCNTs were added to a series of 50 mL conical flasks containing 10 mL of 800 $mg \cdot L^{-1}$ AR solution. The concentration of AR remaining in solution at equilibrium was determined after magnetic separation. The AR adsorption capacity of different materials was explored and the results are shown in Table 2.

Table 2 lists the adsorption of AR by several materials before and after modification. After Fe_3O_4 modification, the adsorption of MCNTs on AR decreased, which was due to the fact that the loading of Fe_3O_4 occupied some of the adsorption sites on the surface of MCNTs. The CS modification provided CMCNTs with a large number of $-NH_2$ and –OH active functional groups, which enhanced the adsorption capacity for anionic AR with a significant increase in the adsorption amount. After

Table 2
Comparison of adsorption capacities of CNTs, MCNTs, CMCNTs, Zr-CMCNTs and Fe_3O_4 on AR.

Absorbent materials	Fe_3O_4	CNTs	MCNTs	CMCNTs	Zr-CMCNTs
$q_e/(mg \cdot g^{-1})$	41.9	90.6	87.7	487	729

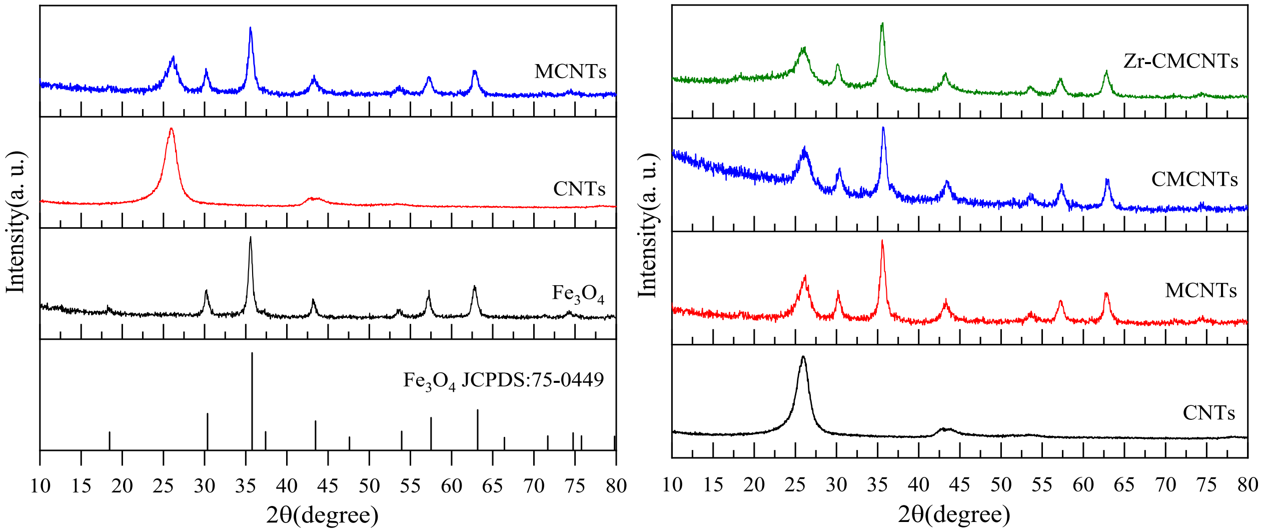

Fig. 4. XRD plots of CNTs, MCNTs, CMCNTs, Zr-CMCNTs and Fe_3O_4.

modification with $ZrOCl_2{\cdot}8H_2O$, the adsorption of AR by the material was again significantly enhanced due to the high affinity of Zr(IV) for AR containing o-dihydroxyl groups, which generates complexation to promote the adsorption process [42].

3.2.2. Effect of pH on the adsorption AR of Zr-CMCNTs

To assess the impact of solution pH on the efficiency of the adsorbent, 10 mg of Zr-CMCNTs were added to a set of 50 mL conical flasks containing 10 mL of 800 $mg{\cdot}L^{-1}$ AR solution at an adjusted pH ranging from 3 to 11. The concentration of AR remaining in solution was determined by constant temperature oscillation at 303 K and magnetic separation after adsorption equilibrium. The effect of pH on the adsorbed AR onto Zr-CMCNTs was explored and the results are shown in Fig. S6.

As shown in Fig. S6, the adsorption of Zr-CMCNTs on AR decreased significantly with the increase of pH. This may be due to the fact that the isoelectric point of Zr-CMCNTs is 4.65, when $pH < 4.65$, the surface of Zr-CMCNTs is positively charged due to the protonation of $-NH_2$, which creates an electrostatic attraction with the AR. Above this pH (i.e. when $pH > 4.65$), there is an increase in the deprotonation of functional groups on the adsorbent causing it to be negatively charged thereby creating an electrostatic repulsion. This may account for the decrease in adsorption efficiency with increasing solution pH [43]. Additionally, as pH increased, OH^- increased and competed with AR for active sites further adversely affecting the adsorption of AR onto Zr-CMNT. At higher pH, Zr-CMCNTs still showed good adsorption capacity for AR, indicating that the adsorption process involves hydrogen bonding or other forces in addition to electrostatic attraction [44]. The AR was still able to maintain a high adsorption capacity of 723 $mg{\bullet}g^{-1}$ at the pH of the stock solution (i.e. $pH = 3.35$), therefore in a bid to further reduce cost and also the ease with working with the solution at its natural pH, $pH = 3.35$ was chosen for the subsequent experiments.

3.2.3. Effect of adsorbent dosage on the adsorption AR of Zr-CMCNTs

The adsorbent dose plays a crucial role in the adsorption studies due to its influence on the number of active sites present for the adsorption process. In this assessment, the dose of Zr-CMCNTs used was varied from 2 to 20 mg. the results from this study as shown in Fig. S7a, indicates that as the adsorbent dosage increases, the adsorption capacity of the material increases but the removal rate decreases. This was due to the increase in the number of adsorbents, which provided more active sites. At fixed AR concentration and varying adsorbent dose, the amount of AR adsorbed onto each active site is reduced leading to a reduction in adsorption capacity with increasing adsorbent dose. Therefore, considering the utilization of Zr-CMCNTs and the removal rate of AR, 10 mg of Zr-CMCNT was selected as the optimum dose and used for subsequent experiments.

3.2.4. Effect of salt concentration on the adsorption AR of Zr-CMCNTs

The effect of salt concentration on the adsorption process was explored by varying the concentrations of either NaCl or Na_2SO_4 present in the system. As shown in Fig. S7b, the adsorption capacity of Zr-CMCNTs towards AR decreased with the increase of salt concentration from 0 to 0.10 $mol{\cdot}L^{-1}$, suggesting that the adsorption process may be characterized by ion exchange or electrostatic attraction. The negative effect of SO_4^{2-} was greater than that of Cl^- due to the fact that AR is an anionic pollutant and the ionic strength of SO_4^{2-} was greater than that of Cl^-, creating more anions to compete with AR for adsorption sites. However, there were still higher value of q_e even at salt concentration 0.10 $mol{\cdot}L^{-1}$, suggesting that Zr-CMCNTs have good salt tolerance and that there may be other forces involved in the adsorption process.

3.2.5. Competitive adsorption studies of AR and AK

In order to demonstrate that the material Zr-CMCNTs has a high affinity for the pollutant AR containing neighboring dihydroxyl groups, the dye AK containing non-neighboring dihydroxyl groups was experimentally selected for competitive adsorption with AR to investigate whether the Zr-CMCNTs are highly selective for AR during the adsorption process. In this assessment, 10 mg of Zr-CMCNTs was added to three sets of 50 mL conical flasks containing 10 mL of 400 $mg{\cdot}L^{-1}$ (containing 0.10 $mol{\cdot}L^{-1}$ NaCl) solution of AR and AK alone, and mixed component solution of AR and AK.

Fig. S8a shows that the competitive adsorption experiments of Zr-CMCNTs towards AR and AK resulted in adsorption capacity of 390 $mg{\cdot}g^{-1}$ and 380 $mg{\cdot}g^{-1}$ for AR and AK alone, whereas the amounts of AR and AK adsorbed in mixed adsorption were 342 $mg{\cdot}g^{-1}$ and 251 $mg{\cdot}g^{-1}$. AR adsorption decreased by 14.4 % and AK by 33.9 %, indicating that Zr-CMCNTs are more selective and easier to bind AR in the mixed solution [45]. The adsorption constants K_d ($K_d = q_e/C_e$) of AR and AK when adsorbed individually were also compared, and it was found that the K_d values were 42.1 for AR and 22.6 for AK, which further confirmed that the Zr-CMCNTs have high affinity for AR and can selectively adsorb AR in mixed pollutant solutions.

The effect of salt concentration on the adsorption efficiency of Zr-CMCNTs towards AR and AK was further explored. In this investigation, 10 mg of Zr-CMCNTs was added to two sets of a series of 50 mL conical flasks containing 10 mL of 400 $mg{\cdot}L^{-1}$ of either AR or AK solutions with varying concentrations of NaCl or Na_2SO_4 in the range of 0–0.10 $mg{\cdot}L^{-1}$. As can be seen from Fig. S8b, the adsorption capacity of Zr-CMCNTs towards both AR and AK decreased with the increase of salt concentration. Also, it was observed that effect of SO_4^{2-} was greater than that of Cl^-, which was due to the fact that the ionic strength of SO_4^{2-} was greater than that of Cl^-, indicating that the adsorption process was all electrostatic attraction. However, the adsorption capacity did not decrease much for AR adsorption in the presence of salt during the adsorption process, indicating that the adsorbent has the good salt resistance.

3.3. Adsorption isotherm, kinetic and thermodynamic analysis

3.3.1. Adsorption isotherm model fit analysis

The influence of the concentration of AR solution on the adsorption capacity of Zr-CMCNTs was assessed by varying its concentration from 500 to 1400 $mg{\cdot}L^{-1}$ and the experiments carried out at 293 K, 303 K and 313 K. From Fig. 5a, it can be seen that the adsorption capacity gradually increased with the increase of AR equilibrium concentration. This was due to more AR molecules being adsorbed by a unit active site on the adsorbent with increasing AR concentration. Additionally, with the increase of temperature, the adsorption of AR on Zr-CMCNTs gradually increased, indicating that the adsorption reaction is a heat-absorbing reaction.

The nonlinear forms of the Langmuir, Freundlich, Koble-Corrigan, and Temkin models were used to fit the obtained experimental data. The fitted curves are shown in Fig. 5a, whereas the associated fitted parameters are listed in Table 3. As shown in Table 3, during the adsorption of AR onto Zr-CMCNTs, the Langmuir model showed that the actual maximum adsorption capacity at 293, 303 and 313 K was 812 $mg{\cdot}g^{-1}$, 875 $mg{\cdot}g^{-1}$ and 889 $mg{\cdot}g^{-1}$, which were similar to the theoretical adsorption amounts. Furthermore, the R^2 values for all temperatures were all >0.946. This indicates the suitability of this model in describing the adsorption process of AR on Zr-CMCNTs and that the adsorption was monomolecular layer adsorption. For the Freundlich isotherm, the $1/n$ values ranged from 0.132 to 0.147, indicating that the adsorption process was feasible and could easily. The observed R^2 values were all >0.927. This observation also confirms the ability of the Freundlich model in describing the adsorption process, suggesting a non-homogeneous phase adsorption on multimolecular layers [46]. The R^2 value in the Temkin model was >0.985, which also suggests its suitability to describe the adsorption process. The Koble-Corrigan model is a three-parameter model, and the value of n tended to be close to 1, indicating that the Langmuir model is more suitable for describing this adsorption process, with a low degree of nonuniformity in the adsorption process and independence between adsorption sites, relative to the

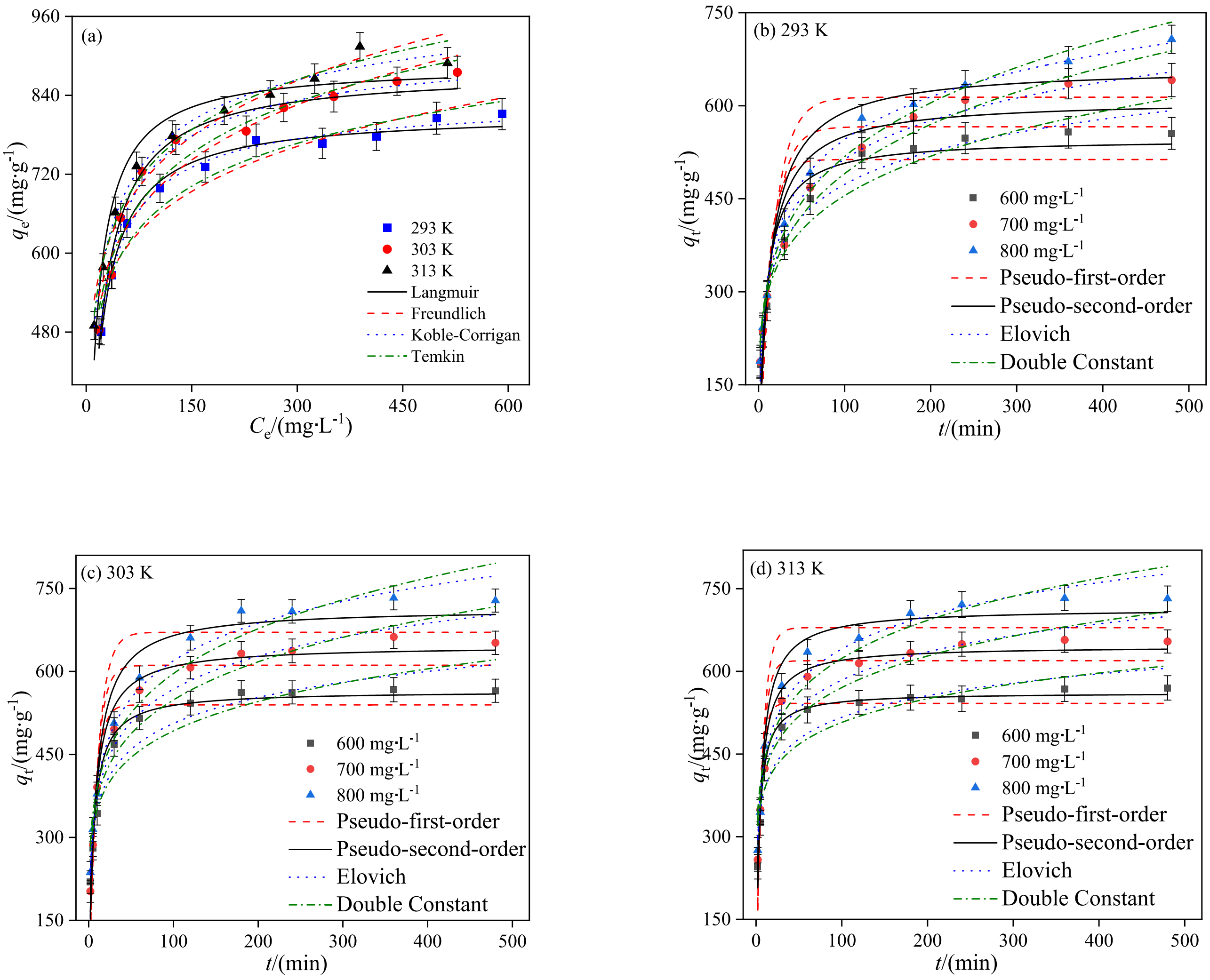

Fig. 5. Adsorption of AR onto Zr-CMCNTs (a. isotherm fits; kinetic fits, b. 293 K, c. 303 K, d. 313 K).

Freundlich model. In addition, the R^2 value was >0.952, indicating that the adsorption process also followed the Koble-Corrigan model. These observations were similar to that made by Yang et al. [47] who utilized pentaerythritol-modified carbon nanotubes for adsorption of organic dyes AR from wastewater. In summary, the adsorption process of Zr-CMCNTs on AR is a complex process that involves both monolayer and multilayer adsorption.

As shown in Table 4, comparing the adsorption of AR by different adsorbents, Zr-CMCNTs showed excellent adsorption performance.

3.3.2. *Adsorption kinetic curve model fitting analysis*

A series of 50 mL conical flasks were taken and 10 mL each of AR solutions with initial concentrations of 600 mg·L^{-1}, 700 mg·L^{-1}, and 800 mg·L^{-1} added. A specified amount of Zr-CMCNTs (i.e. 10 mg) was added, to the conical flasks after which they were oscillated at 293 K, 303 K, and 313 K. At specified times, a conical flask was taken out and the remaining AR solution was determined after the adsorbent was magnetically separated. The results were plotted in terms of adsorbed amount q_t and time t at a certain temperature and are shown in Fig. 5(b, c, d). From the analysis of this data, it can be seen that the adsorption was fast at the initial stages after which it slowed down gradually until equilibrium was reached. This was mainly due to the more active sites on the adsorbent surface at the beginning of the reaction and the reaction proceeded faster. The adsorbed AR on Zr-CMCNT at the studied initial concentrations all increased with increasing temperature, indicating that the adsorption process is a heat-absorbing reaction.

In order to further investigate the underlying adsorption mechanisms, the nonlinear forms of the pseudo-first-order, pseudo-second-order, Elovich and Double constant models were fitted to the kinetic data. The fitted curves from this analysis are shown in Fig. 5 whereas the values for associated kinetic parameters are shown in Table 5. Comparing the R2 values for the four kinetic models, the pseudo-first-order model had a small R^2 value and a large *SSE* value suggesting it not to be suitable in describing the process. The fitting results obtained from the Pseudo-second-order model at the studied temperatures and concentration were however more favorable. The adsorption rate increased nonlinearly with the increase of adsorbent concentration, and the theoretical adsorption capacity was closer to the experimental value. Additionally, the observed R^2 values were all above 0.912, with the *SSE* values relatively small. This may indicate its suitability in describing the adsorption process to a certain extent. This indicates the major role of chemisorption processes underlying the uptake of AR on Zr-CMCNT. The R^2 values obtained from fitting the Elovich and Double constant models were found to be >0.852 with smaller *SSE* values are smaller. This observation indicates that the adsorption is a non-homogeneous phase adsorption process that includes ion exchange. Based on these results, it can be concluded that, the adsorption of AR onto Zr-CMCNTs is a nonhomogeneous chemisorption process.

3.3.3. *Calculation of thermodynamic parameters and apparent activation energy*

In order to study and determine the spontaneity, energy change and

Table 3
Results of isotherm model fitting for adsorption of AR by Zr-CMCNTs.

Langmuir					
T/K	$K_L \times 10^{-2}$/(L·mg^{-1})	$q_{m(exp)}$/(mg·g^{-1})	$q_{m(theo)}$/(mg·g^{-1})	R^2	$SSE \times 10^3$
293	6.47 ± 0.36	812	815 ± 6	0.988	1.30
303	5.89 ± 0.46	875	878 ± 11	0.978	3.49
313	4.48 ± 1.09	889	886 ± 17	0.946	9.54

Freundlich				
T/K	K_F	$1/n$	R^2	$SSE \times 10^3$
293	359 ± 27	0.132 ± 0.014	0.927	0.799
303	347 ± 28	0.152 ± 0.015	0.932	1.53
313	371 ± 21	0.147 ± 0.011	0.963	0.650

Koble-Corrigan					
T/K	A	B	n	R^2	$SSE \times 10^4$
293	97.6 ± 26.4	0.116 ± 0.029	0.804 ± 0.086	0.993	0.782
303	109 ± 39	0.118 ± 0.039	0.757 ± 0.118	0.985	2.24
313	265 ± 48	0.251 ± 0.032	0.505 ± 0.077	0.991	1.59

Temkin				
T/K	A	B	R^2	$SSE \times 10^3$
293	239 ± 38	92.5 ± 7.3	0.952	5.21
303	194 ± 41	111 ± 8	0.958	6.57
313	243 ± 25	109 ± 5	0.983	3.90

Notice: $SSE = \sum (q_c - q_e)^2$, q_c is the predicted (calculated) data with the isotherm equations and q_e is the experimental data.

Table 4
Comparison of AR adsorption capacity of Zr-CMCNTs with reported materials.

Adsorbents	q_e/(mg·g^{-1})	Reference
Fe-BTC	80.0	[56]
Magnetic chitosan	201	[57]
PEI@MCNTs	196	[58]
Zr-CMCNTs	889	This study

disorder of the adsorption process, the change in Gibbs free energy (ΔG), enthalpy change (ΔH) and entropy change (ΔS) were calculated based on the experimental data. The formulae for each parameter are given below [48]:

$$K_{eq} = q_e / C_e \tag{5}$$

$$\Delta G = -R\,T\ln K_{eq}' \tag{6}$$

$$\Delta G = \Delta H - T\Delta S \tag{7}$$

In the above equation, q_e is the equilibrium adsorption capacity (mg·g^{-1}), C_e is the concentration of pollutant remaining in solution at equilibrium (mg·L^{-1}), R is the ideal gas constant (8.314 J·mol^{-1}·K^{-1}), and T is the temperature of the adsorption reaction (K).

The ease with which an adsorption reaction can take place is expressed by the thermodynamic parameter, apparent activation energy E_a. E_a values between 5 and 40 kJ·mol^{-1} are considered physical adsorption, and adsorption >40 kJ·mol^{-1} is considered chemical adsorption. The smaller the value of activation energy, the faster the reaction rate and the adsorption is more likely to occur. The expression is given below:

$$\ln K = -\frac{E_a}{RT} + \ln A \tag{8}$$

In the above equation, A is the temperature influence factor, K is the adsorption rate constant, and T is the reaction temperature (K).

The thermodynamic parameters and apparent activation energies of Zr-CMCNTs loaded AR were calculated according to the above Eq. (5–8), and the results are shown in Table 6. As shown in Table 6, the ΔG values were $-$ 0.744 kJ·mol^{-1}, −1.25 kJ·mol^{-1}, and $-$ 1.44 kJ·mol^{-1} at 293, 303 and 313 K respectively. This shows that the reaction proceeded spontaneously and involved physical adsorption. Additionally, $\Delta H > 0$ and $\Delta S > 0$ indicated that the adsorption process was an entropy increasing heat absorption reaction process. The ΔH values ranged between −20–40 kJ·mol^{-1} indicating that the adsorption processes were involved physisorption processes [49]. Also, the calculated E_a value was small and the reaction was easy to occur.

3.4. *Desorption and regeneration of adsorbent Zr-CMCNTs*

The results to assess the reusability efficiency of Zr-CMCNT is shown in Fig. 6. It was evident from this figure that 0.1 mol·L^{-1} NaOH as an eluent achieved the best desorption (i.e. 80.4 %) and regeneration efficiency of the adsorbent. The high desorption rate associated with the use of this eluent may be attributed to the fact that AR is an anionic pollutant thus may compete with the generated OH$^-$ for adsorption sites [50]. After three cycles of desorption and regeneration, the Zr-CMCNT still had good regeneration ability, and the regeneration rate was still as high as 60.7 %, which indicates its good reusability property. This feature of adsorbents usually promotes the prospects of adsorbents for practical remediation of wastewater due to their associated economic benefits.

3.5. *XPS analysis and mechanism study*

In order to further investigate the mechanism of AR adsorption by Zr-CMCNTs, the materials before and after adsorption were characterized

Table 5
Results of nonlinear fitting of kinetic curves for adsorption of AR by Zr-CMCNTs.

Pseudo-first-order

T/K	C_0/(mg·L^{-1})	$q_{e(exp)}$/(mg·g^{-1})	$q_{e(theo)}$/(mg·g^{-1})	k_1/(min^{-1})	R^2	$SSE\times10^4$
293	600	555	516 ± 25	0.088 ± 0.022	0.836	3.11
	700	641	572 ± 34	0.063 ± 0.020	0.797	5.40
	800	707	613 ± 35	0.057 ± 0.017	0.822	5.66
303	600	565	540 ± 19	0.135 ± 0.024	0.881	1.88
	700	652	612 ± 21	0.114 ± 0.021	0.904	2.36
	800	728	671 ± 32	0.097 ± 0.024	0.836	5.16
313	600	570	541 ± 13	0.199 ± 0.027	0.910	1.03
	700	652	618 ± 20	0.158 ± 0.027	0.881	2.20
	800	732	680 ± 25	0.141 ± 0.027	0.867	3.37

Pseudo-second-order

T/K	C_0/(mg·L^{-1})	$q_{e(exp)}$/(mg·g^{-1})	$q_{e(theo)}$/(mg·g^{-1})	$k_2\times10^{-4}$/ (g·mg^{-1}·min^{-1})	R^2	$SSE\times10^4$
293	600	555	549 ± 18	2.28 ± 0.50	0.939	1.15
	700	641	614 ± 28	1.50 ± 0.43	0.912	2.34
	800	707	659 ± 29	1.26 ± 0.34	0.924	2.42
303	600	565	565 ± 11	3.61 ± 0.50	0.967	0.513
	700	652	647 ± 12	2.46 ± 0.30	0.979	0.515
	800	728	715 ± 23	1.88 ± 0.39	0.942	1.82
313	600	570	561 ± 6	5.69 ± 0.45	0.987	0.153
	700	652	646 ± 11	3.74 ± 0.45	0.974	0.487
	800	732	714 ± 16	2.87 ± 0.44	0.960	1.01

Elovich

T/K	C_0/(mg·L^{-1})	A	B	R^2	$SSE\times10^3$
293	600	124 ± 17	75.7 ± 3.9	0.979	3.96
	700	99.0 ± 13.6	90.1 ± 3.1	0.990	2.55
	800	90.7 ± 12.4	98.7 ± 2.8	0.993	2.09
303	600	194 ± 25	67.7 ± 5.8	0.945	8.59
	700	174 ± 24	85.6 ± 5.6	0.967	8.21
	800	169 ± 18	97.7 ± 4.2	0.986	4.53
313	600	256 ± 28	56.7 ± 6.5	0.905	10.9
	700	246 ± 26	73.7 ± 5.9	0.951	9.11
	800	240 ± 24	86.9 ± 5.6	0.968	8.01

Double constant

T/K	C_0/(mg·L^{-1})	A	Ks	R^2	$SSE\times10^4$
293	600	193 ± 19	0.186 ± 0.019	0.943	1.08
	700	182 ± 13	0.215 ± 0.013	0.979	0.552
	800	185 ± 12	0.224 ± 0.013	0.983	0.551
303	600	250 ± 26	0.147 ± 0.021	0.892	1.70
	700	252 ± 28	0.169 ± 0.022	0.911	2.18
	800	257 ± 23	0.183 ± 0.018	0.949	1.59
313	600	297 ± 28	0.117 ± 0.019	0.852	1.70
	700	303 ± 28	0.138 ± 0.018	0.900	1.85
	800	310 ± 28	0.151 ± 0.017	0.923	1.94

Table 6
Thermodynamic parameters of adsorbed AR by Zr-CMCNTs.

E_a/ (kJ·mol^{-1})	ΔH/ (kJ·mol^{-1})	ΔS/ (J·mol^{-1}·K^{-1})	ΔG/(kJ·mol^{-1})		
			293 K	303 K	313 K
31.4	11.1	40.4	−0.744	−1.25	−1.44

and analyzed by XPS, and the full spectrum is shown in Fig. 7. A high-resolution analysis of major elements before and after the adsorption process was also carried out and the results shown in Fig. 8. As can be seen in Fig. 7, Zr-CMCNTs contained five elements, C, O, N, Fe and Zr. The Fe element came from the magnetic particles Fe_3O_4, and the Zr element came from $ZrOCl_2\cdot8H_2O$, which indicated that the material was successfully synthesized. The S 2p characteristic peak appeared after the adsorption of AR onto Zr-CMCNTs, which indicated that AR was successfully adsorbed onto the surface of the material.

From Fig. 8a, the detailed analysis of C 1 s before adsorption could be deconvoluted into three peaks at 284.23 eV, 285.91 eV and 287.92 eV corresponding to C=C/C–C, C—O and C═O bonds [51]. The split peak representing the benzene ring C═C shifted from 284.23 eV to 284.25 eV, which may be attributed to the interaction between the conjugated large π-bonds in the CNTs and the aromatic ring of AR, suggesting the presence of π-π stacking. As can be seen from Fig. 8b, before adsorption O 1 s could be split into three peaks at 530.3 eV, 531.45 eV, and 532.9 eV, which represented O^{2-}, C═O, and C—O bonds, respectively. The position of C═O and C—O peaks shifted and with associated changes in their peak area after adsorption of AR. This was because the protonated amino groups (-NH_3^+) on the surface of Zr-CMCNTs attracted the negatively charged sulfonic acid groups and carbonyl groups in AR molecules, increasing the surface C═O density and thus the peak area,

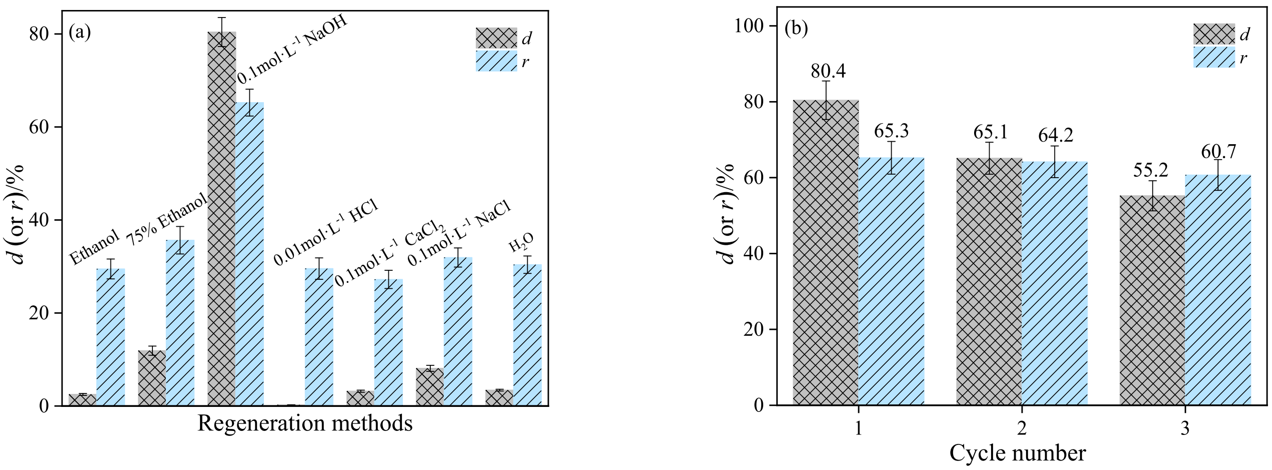

Fig. 6. Desorption and regeneration of Zr-CMCNTs after adsorption of AR (a. Comparison of different desorption solutions, b. Three times desorption and regeneration with 0.01 mol·L^{-1} NaOH).

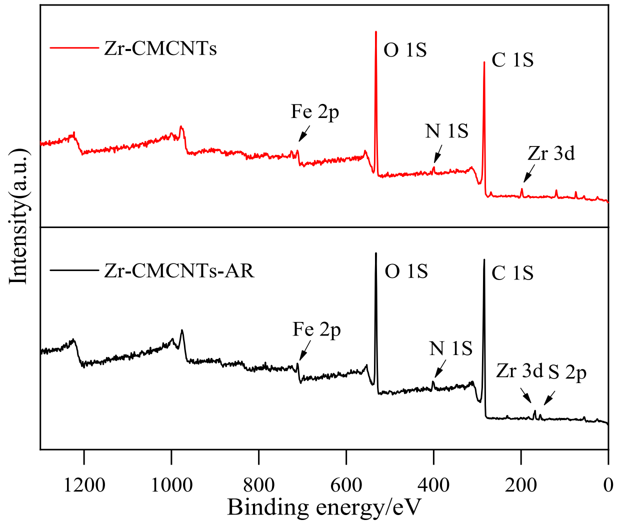

Fig. 7. Full XPS spectra of Zr-MCNTs before and after adsorption of AR.

indicating the presence of electrostatic attraction. Additionally, the amino (-NH₂) or hydroxyl (-OH) groups in chitosan formed hydrogen bonds with the carbonyl groups (C=O) in AR, causing AR molecules to be adsorbed onto the material surface via hydrogen bonding and leading to an increase in the C=O peak area, which suggested the existence of hydrogen bonding [52]. The peak area of O^{2-} increased significantly from 9.46 % to 14.4 %. Zr formed stable coordination bonds with the adjacent dihydroxyl groups (-OH) in AR molecules, leading to the increase in the O^{2-} peak area, indicating the presence of complexation. As can be seen from Fig. 8c, before adsorption, N 1 s was deconvoluted into two peaks ascribed to –NH$_2$ and –NH$_3^+$/–NH$_2^+$ with binding energies of 402.5 and 399.83 eV, respectively. After adsorption, the area of the –NH$_2$ peak decreased significantly, whereas the area of the –NH$_3^+$/–NH$_2^+$ peak increased from 39.3 to 48.4 %, indicating that during adsorption, the adsorbent surface –NH$_2$ was protonated interacted with AR via electrostatic attraction [53]. As can be seen from Fig. 8d, before adsorption, Zr 3d was split into two peaks representing Zr—O bonding, corresponding to Zr 3d$_{5/2}$ Zr 3d$_{3/2}$, with binding energies of 185.17 eV and 182.82 Ev [54]. After adsorption, the area of the peaks decreased significantly after adsorption, and the area of the O^{2-} peak in the bound O 1 s increased, and which indicated that there was complexation in the adsorption process [55]. Based on these analyses, the adsorption of AR onto Zr-CMCNT involved complexation, hydrogen bonding, π-π stacking, and electrostatic attraction mainly existed during the adsorption of Zr-CMCNTs to AR. A schematic diagram showing the underlying mechanisms involved in the uptake of AR onto Zr-CMCNT is shown in Fig. 9.

4. Conclusion

Multiple modification approach was used to synthesize a powerful adsorbent material for anionic pollutants. Zr-CMCNTs was fabricated with carbon nanotubes functionalized using Fe_3O_4, chitosan, and zirconium. The performance of Zr-CMCNTs was assessed using AR as a model pollutant. The maximum adsorption of Zr-CMCNTs on AR at 313 K was 889 mg·g^{-1} (pH = 3.4), indicating a high adsorption efficiency. In the presence of common ions, the adsorption of Zr-CMCNTs was still 532.96 mg·g^{-1}, indicating good salt tolerance. In the competition adsorption experiment with AK, the adsorbed amount of AR was reduced by 14.4 %, indicating Zr-CMCNTs' selectivity towards AR. After three cycles of desorption and regeneration, Zr-CMCNTs still obtained a regeneration rate of 60.7 % indicating a good reusability. Langmuir, Freundlich, Koble-Corrigan and Temkin models could describe the adsorption isotherm, indicating the presence of monolayer and multilayer adsorption. Adsorption kinetics fitted pseudo-second-order, Elovich and Double constant kinetic models, suggesting that nonhomogeneous chemisorption dominated. Thermodynamic studies indicated that the adsorption of AR on Zr-CMCNTs was a spontaneous, entropy-increasing, and endothermal process. The adsorption mechanisms are mainly complexation, hydrogen bonding, π-π stacking and electrostatic attraction. In summary, Zr-CMCNTs has great potential for removing anionic organic pollutants from wastewater.

CRediT authorship contribution statement

Jing Jin: Writing – original draft, Visualization, Methodology, Investigation, Formal analysis, Conceptualization. **Hanyu Zhang:** Writing – original draft, Methodology, Formal analysis, Conceptualization. **Aaron Albert Aryee:** Writing – review & editing, Formal analysis, Conceptualization. **Yuanyuan Wang:** Methodology, Formal analysis. **Rashda safdar:** Methodology, Formal analysis. **Weimin Shi:** Supervision, Formal analysis, Conceptualization. **Lingbo Qu:** Supervision, Funding acquisition. **Runping Han:** Writing – review & editing, Visualization, Supervision, Conceptualization.

Declaration of competing interest

The authors declare that they have no known competing financial

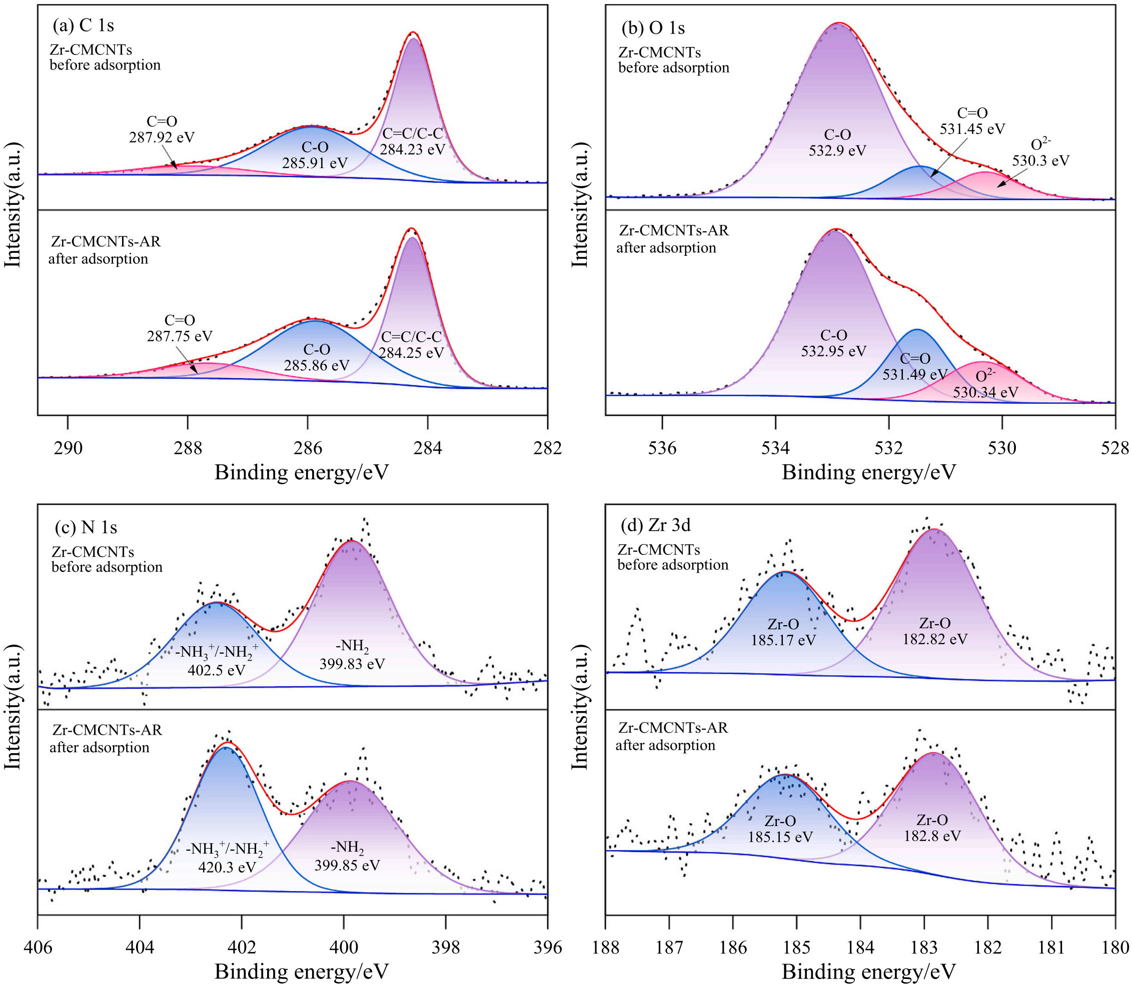

Fig. 8. Comparison of XPS spectra of Zr-CMCNTs before and after adsorption of AR.

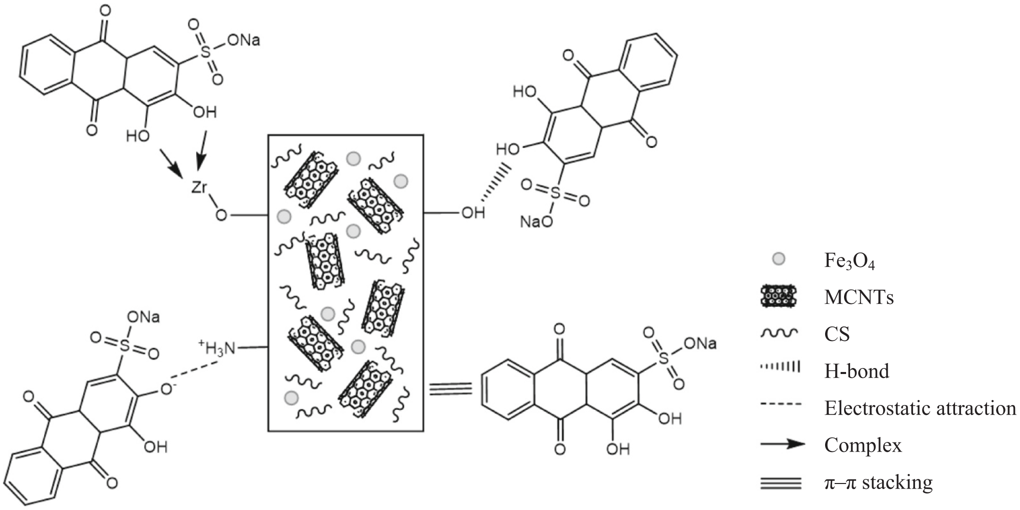

Fig. 9. Mechanism of AR adsorption onto Zr-CMCNTs.

interests or personal relationships that could have appeared to influence the work reported in this paper.

Acknowledgements

The research was supported by Zhongyuan Scholars Foundation (202101510005).

Appendix A. Supplementary data

Supplementary data to this article can be found online at https://doi.org/10.1016/j.ijbiomac.2025.144779.

Data availability

Data will be made available on request.

References

[1] K. Smith, S. Liu, Y. Liu, S. Guo, Can China reduce energy for water? A review of energy for urban water supply and wastewater treatment and suggestions for change, Renew. Sust. Energ. Rev. 91 (2018) 41–58, https://doi.org/10.1016/j.rser.2018.03.051.

[2] R. Garg, R. Sabouni, A. Alaamer, A. Alali, D. Al-Muqbel, H. Alqassem, K. Almazrooei, Recent development in metal-organic framework-based hybrid nanocomposites for pollutants remediation from wastewater: challenges and opportunities, Environ. Technol. 32 (2023) 103446, https://doi.org/10.1016/j.eti.2023.103446.

[3] D. Machiwal, M.K. Jha, V.P. Singh, C. Mohan, Assessment and mapping of groundwater vulnerability to pollution: current status and challenges, Earth Sci. Rev. 185 (2018) 901–927, https://doi.org/10.1016/j.earscirev.2018.08.009.

[4] H. Abdipour, A. Azari, H. Kamani, K. Pirasteh, F.K. Mostafapour, S. Rayegnnakhost, Human health risk assessment for fluoride and nitrate contamination in drinking water of municipal and rural areas of Zahedan, Iran, Appl Water Sci 15 (2025) 47, https://doi.org/10.1007/s13201-025-02375-8.

[5] D. Azizi, A. Arif, D. Blair, J. Dionne, Y. Filion, Y. Ouarda, A.G. Pazmino, R. Pulicharla, V. Rilstone, B. Tiwari, L. Vignale, S.K. Brar, P. Champagne, P. Drogui, V.S. Langlois, J.F. Blais, A comprehensive review on current technologies for removal of endocrine disrupting chemicals from wastewaters, Environ. Res. 207 (2022) 112196, https://doi.org/10.1016/j.envres.2021.112196.

[6] X.F. Gao, S. Kang, R.W. Xiong, M. Chen, Environment-friendly removal methods for endocrine disrupting chemicals, Sustainability 12 (2020) 7615, https://doi.org/10.3390/su12187615.

[7] K.K. Nejumal, M.I. Satayev, M.P. Rayaroth, P. Arun, D. Dineep, U.K. Aravind, A. M. Azimov, C.T. Aravindakumar, Degradation studies of bisphenol S by ultrasound activated persulfate in aqueous medium, Ultrason. Sonochem. 101 (2023) 106700, https://doi.org/10.1016/j.ultsonch.2023.106700.

[8] S. Sessarego, S.C.G. Rodrigues, Y. Xiao, Q.Y. Lu, J.M. Hill, Phosphonium-enhanced chitosan for Cr(VI) adsorption in wastewater treatment, Carbohydr. Polym. 211 (2019) 249–256, https://doi.org/10.1016/j.carbpol.2019.02.003.

[9] G.L. Dotto, G. McKay, Current scenario and challenges in adsorption for water treatment, J. Environ. Chem. Eng. 8 (2020) 103988, https://doi.org/10.1016/j.jece.2020.10.3988.

[10] J.B. Guo, H. Jiang, Y. Teng, Y. Xiong, Z.H. Chen, L.J. You, D.L. Xiao, Recent advances in magnetic carbon nanotubes: synthesis, challenges and highlighted applications, J. Mater. Chem. B 9 (2021) 9076–9099, https://doi.org/10.1039/d1tb01242h.

[11] J.-Y. Yang, X.-Y. Jiang, F.-P. Jiao, J.-G. Yu, The oxygen-rich pentaerythritol modified multi-walled carbon nanotube as an efficient adsorbent for aqueous removal of alizarin yellow R and alizarin red S, Appl. Surf. Sci. 436 (2018) 198–206, https://doi.org/10.1016/j.apsusc.2017.12.029.

[12] I.A. Lawal, M.M. Lawal, S.O. Akpotu, M.A. Azeez, P. Ndungu, B. Moodley, Theoretical and experimental adsorption studies of sulfamethoxazole and ketoprofen on synthesized ionic liquids modified CNTs, Ecotoxicol. Environ. Saf. 161 (2018) 542–552, https://doi.org/10.1016/j.ecoenv.2018.06.019.

[13] M. Li, X. Jia, L. Wang, G.Y. Gao, X.F. Feng, C.Y. Li, Research on modified carbon nanotubes in wastewater treatment, Catalysts 12 (2022) 1103, https://doi.org/10.3390/catal12101103.

[14] F. Rabiee, S. Maryam, A. Shohreh, J. Anis, H.S. Yaser, B. Mansour, G. Mitra, A. Azari, The superior decomposition of 2,4-Dinitrophenol under ultrasound-assisted Fe3O4@TiO2 magnetic nanocomposite: process modeling and optimization, effect of various oxidants and degradation pathway studies, Int. J. Environ. Anal. Chem. 104 (2024) 1243–1265, https://doi.org/10.1080/03067319.2022.2034798.

[15] R. Foroutan, S.J. Peighambardoust, Z. Esvandi, H. Khatooni, B. Ramavandi, Evaluation of two cationic dyes removal from aqueous environments using CNT/MgO/CuFe2O4 magnetic composite powder: a comparative study, J. Environ. Chem. Eng. 9 (2021) 104752, https://doi.org/10.1016/j.jece.2020.104752.

[16] S. Liu, J. Wang, Exploring the potential of cellulose benzoate adsorbents modified with carbon nanotubes and magnetic carbon nanotubes for microplastic removal from water, Chem. Eng. J. 469 (2023) 143910, https://doi.org/10.1016/j.cej.2023.143910.

[17] M.A. Khapre, S. Pandey, R.M. Jugade, Glutaraldehyde-cross-linked chitosan-alginate composite for organic dyes removal from aqueous solutions, Int. J. Biol. Macromol. 190 (2021) 862–875, https://doi.org/10.1016/j.ijbiomac.2021.09.026.

[18] M.S. Rostami, M.M. Khodaei, Recent advances in chitosan-based nanocomposites for adsorption and removal of heavy metal ions, Int. J. Biol. Macromol. 270 (2024) 132386, https://doi.org/10.1016/j.ijbiomac.2024.132386.

[19] L. Hevira, J.O. Ighalo, D. Sondari, Chitosan-based polysaccharides for effective synthetic dye adsorption, J. Mol. Liq. 393 (2024) 123604, https://doi.org/10.1016/j.molliq.2023.123604.

[20] Y.F. Gu, M.M. Yang, W.L. Wang, R.P. Han, Phosphate adsorption from solution by zirconium-loaded carbon nanotubes in batch mode, J. Chem. Eng. Data 64 (2019) 2849–2858, https://doi.org/10.1021/acs.jced.9b00214.

[21] J. Peng, Y. He, C. Zhou, S. Su, B. Lai, The carbon nanotubes-based materials and their applications for organic pollutant removal: a critical review, Chin. Chem. Lett. 32 (2021) 1626–1636, https://doi.org/10.1016/j.cclet.2020.10.026.

[22] H.H. Gao, X.Y. Han, R. Wang, K.K. Zhu, R.P. Han, Adsorption and catalytic degradation of bisphenol a and p-chlorophenol by magnetic carbon nanotubes, Environ. Res. 231 (2023) 116314, https://doi.org/10.1016/j.envres.2023.116314.

[23] S. Wang, Y.Y. Zhai, Q. Gao, W.J. Luo, H. Xia, C.G. Zhou, Highly efficient removal of acid red 18 from aqueous solution by magnetically retrievable chitosan/carbon nanotube: batch study, isotherms, kinetics, and thermodynamics, J. Chem. Eng. Data 59 (2014) 39–51, https://doi.org/10.1021/je400700c.

[24] E. Dovi, A.A. Aryee, M.Y. Liu, X.T. Zhang, A.N. Kani, J.J. Li, R.P. Han, L.B. Qu, Biocomposite based on zirconium and amine-grafted walnut shell with antibacterial properties for the removal of alizarin red in water: batch and column studies, Environ. Sci. Pollut. Res. 29 (2022) 90530–90548, https://doi.org/10.1007/s11356-022-22081-1.

[25] M. Abewaa, E. Adino, A. Mengistu, Preparation of Rumex abyssinicus based biosorbent for the removal of methyl orange from aqueous solution, Heliyon 9 (2023) e22447, https://doi.org/10.1016/j.heliyon.2023.e22447.

[26] Y.R. Wang, Q. Yang, Y.N. Du, H.Q. Chen, Chitosan can improve the storage stability of ovalbumin fibrils at pH higher than isoelectric point, Food Hydrocoll. 136 (2023) 108286, https://doi.org/10.1016/j.foodhyd.2022.108286.

[27] M.Y. Liu, Q. Liu, Z.Y. Zang, R.P. Han, Adsorptive removal of sulfosalicylic acid from aqueous medium by iron (III)-loaded magnetic chitosan/graphene oxide, J. Colloid Interface Sci. 606 (2022) 1249–1260, https://doi.org/10.1016/j.jcis.2021.08.097.

[28] E.-J. Lee, H.-S. Kim, U.S. Shin, Wettability control on chitosan-wrapped carbon nanotube surface through simple Octanal-treatment: selective removing phenol from water, Macromol. Res. 24 (2016) 429–435, https://doi.org/10.1007/s13233-016-4055-z.

[29] Z.B. Wang, W.B. Xu, F.H. Jie, Z.W. Zhao, K. Zhou, H. Liu, The selective adsorption performance and mechanism of multiwall magnetic carbon nanotubes for heavy metals in wastewater, Sci. Rep. 11 (2021) 16878, https://doi.org/10.1038/s41598-021-96465-7.

[30] J.S. Liu, W.X. Liu, Y.R. Wang, M.J. Xu, B. Wang, A novel reusable nanocomposite adsorbent, xanthated Fe_3O_4-chitosan grafted onto graphene oxide, for removing cu (II) from aqueous solutions, Appl. Surf. Sci. 367 (2016) 327–334, https://doi.org/10.1016/j.apsusc.2016.01.176.

[31] L.G. Zhang, J.S. Pan, L. Liu, K. Song, Q.L. Wang, Combined physical and chemical activation of sludge-based adsorbent enhances Cr(VI) removal from wastewater, J. Clean. Prod. 238 (2019) 117904, https://doi.org/10.1016/j.jclepro.2019.117904.

[32] A. Abuessawy, A. Fouda, A.A.H. Abdel-Rahman, M.A. Hawata, N.A. Hamad, A new modified heterocyclic-magnetite chitosan nanocomposite for efficient alizarin red dye removal: adsorption analysis and antibacterial activity, J. Polym. Environ. 32 (2024) 826–841, https://doi.org/10.1007/s10924-023-03002-w.

[33] R. Khakpour, H. Tahermansouri, Synthesis, characterization and study of sorption parameters of multi-walled carbon nanotubes/chitosan nanocomposite for the removal of picric acid from aqueous solutions, Int. J. Biol. Macromol. 109 (2018) 598–610, https://doi.org/10.1016/j.ijbiomac.2017.12.105.

[34] S.Y. Zhang, W.L. Li, H.J. Wu, J. Jiao, Multi-optimized flexible graphene oxide/multi-walled carbon nanotubes/ferroferric oxide nanopaper with enhanced electromagnetic wave absorption performance, Adv. Compos. Hybrid Mater. 6 (2023) 154, https://doi.org/10.1007/s42114-023-00736-y.

[35] K.S.W. Sing, R.T. Williams, Physisorption hysteresis loops and the characterization of nanoporous materials, Adsorpt. Sci. Technol. 22 (2004) 773–782, https://doi.org/10.1260/0263617053499032.

[36] M. Thommes, K. Kaneko, A.V. Neimark, J.P. Olivier, F. Rodriguez-Reinoso, J. Rouquerol, K.S.W. Sing, Physisorption of gases, with special reference to the evaluation of surface area and pore size distribution (IUPAC technical report), Pure Appl. Chem. 87 (2015) 1051–1069, https://doi.org/10.1515/pac-2014-1117.

[37] R. Zhang, Y.H. Li, J.J. Yan, J.X. Zeng, Y. Liu, M.M. Zhang, P.F. Liu, X.P. Huang, E. R. Zhang, K.P. Cheng, J.Y. Chen, J.L. Sun, Surface modification of PVDF membranes with quaternized chitosan for selective separation of negatively charged polysaccharides - exemplified with heparin, J. Environ. Chem. Eng. 11 (2023) 110666, https://doi.org/10.1016/j.jece.2023.110666.

[38] H. Esmaeili, S.M. Mousavi, S.A. Hashemi, W.H. Chiang, S.A. Abnavi, Activated carbon@MgO@Fe_3O_4 as an efficient adsorbent for as (III) removal, Carbon Lett. 31 (2021) 851–862, https://doi.org/10.1007/s42823-020-00186-2.

[39] Y. Liu, Z.P. Zhao, D.Z. Yuan, Y. Wang, Y. Dai, J.W. Chew, Fast and high amount of U(VI) uptake by functional magnetic carbon nanotubes with phosphate group, Ind. Eng. Chem. Res. 57 (2018) 14551–14560, https://doi.org/10.1021/acs.iecr.8b03864.

[40] R.R.C. Monteiro, P.J.M. Lima, B.B. Pinheiro, T.M. Freire, L.M.U. Dutra, P.B. A. Fechine, L.R.B. Gonçalves, M.C.M. de Souza, J.C.S. dos Santos, R. Fernandez-Lafuente, Immobilization of lipase a from *Candida antarctica* onto chitosan-coated magnetic nanoparticles, Int. J. Mol. Sci. 20 (2019) 4018, https://doi.org/10.3390/ijms20164018.

[41] M. Farrokhi-Rad, T. Shahrabi, S. Mahmoodi, S. Khanmohammadi, Electrophoretic deposition of hydroxyapatite-chitosan-CNTs nanocomposite coatings, Ceram. Int. 43 (2017) 4663–4669, https://doi.org/10.1016/j.ceramint.2016.12.139.

[42] M.Y. Liu, Z.Y. Zang, S.S. Zhang, G.F. Ouyang, R.P. Han, Enhanced fluoride adsorption from aqueous solution by zirconium (IV)-impregnated magnetic

chitosan graphene oxide, Int. J. Biol. Macromol. 182 (2021) 1759–1768, https://doi.org/10.1016/j.ijbiomac.2021.05.116.

[43] L.P. Mei, J. Wei, R.R. Yang, F. Ke, C.Y. Peng, R.Y. Hou, J.S. Liu, X.C. Wan, H.M. Cai, Zirconium/lanthanum-modified chitosan/polyvinyl alcohol composite adsorbent for rapid removal of fluoride, Int. J. Biol. Macromol. 243 (2023) 125155, https://doi.org/10.1016/j.ijbiomac.2023.125155.

[44] F.M. Machado, S.A. Carmalin, E.C. Lima, S.L.P. Dias, L.D.T. Prola, C. Saucier, I. M. Jauris, I. Zanella, S.B. Fagan, Adsorption of alizarin red S dye by carbon nanotubes: an experimental and theoretical investigation, J. Phys. Chem. C 120 (2016) 18296–18306, https://doi.org/10.1021/acs.jpcc.6b03884.

[45] M.S. Embaby, S.D. Elwany, W. Setyaningsih, M.R. Saber, The adsorptive properties of UiO-66 towards organic dyes: a record adsorption capacity for the anionic dye alizarin red S, Chin. J. Chem. Eng. 26 (2018) 731–739, https://doi.org/10.1016/j.cjche.2017.07.014.

[46] K.Y. Wu, J.G. Yu, X.Y. Jiang, Multi-walled carbon nanotubes modified by polyaniline for the removal of alizarin yellow R from aqueous solutions, Adsorpt. Sci. Technol. 36 (2018) 198–214, https://doi.org/10.1177/0263617416687564.

[47] J.Y. Yang, X.Y. Jiang, F.P. Jiao, J.G. Yu, The oxygen-rich pentaerythritol modified multi-walled carbon nanotube as an efficient adsorbent for aqueous removal of alizarin yellow R and alizarin red S, Appl. Surf. Sci. 436 (2018) 198–206, https://doi.org/10.1016/j.apsusc.2017.12.029.

[48] E.C. Lima, A. Hosseini-Bandegharaei, J.C. Moreno-Piraján, I. Anastopoulos, A critical review of the estimation of the thermodynamic parameters on adsorption equilibria. Wrong use of equilibrium constant in the Van't hoof equation for calculation of thermodynamic parameters of adsorption, J. Mol. Liq. 273 (2019) 425–434, https://doi.org/10.1016/j.molliq.2018.10.048.

[49] Y.D. Liang, Y.J. He, Y.H. Zhang, Q.Q. Zhu, Adsorption property of alizarin red S by $NiFe_2O_4$/polyaniline magnetic composite, J. Environ. Chem. Eng. 6 (2018) 416–425, https://doi.org/10.1016/j.jece.2017.12.022.

[50] J.F. Zhou, Y.Q. Sun, C.Q. Zhou, X.H. Sun, J. Han, Polyaniline/carbon hybrids: synthesis and application for alizarin red S removal from water, Colloids Surf. A Physicochem. Eng. Aspects 676 (2023) 132204, https://doi.org/10.1016/j.colsurfa.2023.132204.

[51] B. Moeini, M.R. Linford, N. Fairley, A. Barlow, P. Cumpson, D. Morgan, V. Fernandez, J. Baltrusaitis, Definition of a new (Doniach-Sunjic-Shirley) peak shape for fitting asymmetric signals applied to reduced graphene oxide/graphene oxide XPS spectra, Surf. Interface Anal. 54 (2022) 67–77, https://doi.org/10.1002/sia.7021.

[52] H.M. Agha, A.H. Jawad, L.D. Wilson, K. Al-Essa, Z.A. Alothman, A *chitosan-Staphylococcus epidermidis* bacterial biocomposite adsorbent for removal of reactive orange 16 dye: box-Behnken design optimization, Int. J. Biol. Macromol. 309 (2025) 142752, https://doi.org/10.1016/j.ijbiomac.2025.142752.

[53] F.L. Liu, Z.D. Zhou, G.Y. Li, Persimmon tannin functionalized polyacrylonitrile fiber for highly efficient and selective recovery of au(III) from aqueous solution, Chemosphere 264 (2021) 128469, https://doi.org/10.1016/j.chemosphere.2020.128469.

[54] B.Y. Liu, N.D. Guo, Z. Wang, Y. Wang, X. Hao, Z.L. Yang, Q. Yang, Adsorption of 2,4-dichlorophenoxyacetic acid over Fe-Zr-based metal-organic frameworks: synthesis, characterization, kinetics, and mechanism studies, J. Environ. Chem. Eng. 10 (2022) 107472, https://doi.org/10.1016/j.jece.2022.107472.

[55] M.Y. Liu, X.T. Zhang, Z.H. Li, L.B. Qu, R.P. Han, Fabrication of zirconium (IV)-loaded chitosan/Fe_3O_4/graphene oxide for efficient removal of alizarin red from aqueous solution, Carbohydr. Polym. 248 (2020) 116792, https://doi.org/10.1016/j.carbpol.2020.116792.

[56] G.R. Delpiano, D. Tocco, L. Medda, E. Magner, A. Salis, Adsorption of malachite green and alizarin red S dyes using Fe-BTC metal organic framework as adsorbent, Int. J. Mol. Sci. 22 (2021) 788, https://doi.org/10.3390/ijms22020788.

[57] S.S. Vedula, G.D. Yadav, Treatment of wastewater containing alizarin red dye: development and application of magnetic chitosan as a natural eco-friendly material, Clean Techn. Environ. Policy 25 (2023) 865–878, https://doi.org/10.1007/s10098-022-02408-9.

[58] Z.F. Zhang, H.J. Chen, W.M. Wu, W.T. Pang, G.Q. Yan, Efficient removal of alizarin red S from aqueous solution by polyethyleneimine functionalized magnetic carbon nanotubes, Bioresour. Technol. 293 (2019) 122100, https://doi.org/10.1016/j.biortech.2019.122100.